Journal of Engineering and Computer Sciences
Qassim University, Vol. 5, No. 1, pp. 53-76 (January 2012/Safar 1433H)

Frost Formation and Heat Transfer over Flat Plate Evaporator

G.I. Sultan[*a,b], E. A. ElShafiee[a], M. G. Safan[a], M. A. Elraouf
[a] *Mansoura University, Faculty of Engineering, Mansoura, Egypt*
[b] *Qassim University, Faculty of engineering, Burydah, Saudi Arabia*
Email: gisultan@mans.edu.eg

(Received 2/3/2011; accepted for publication 24/2/2012)

ABSTRACT. In the present study, numerical and experimental investigations of heat and mass transfer characteristics of a plate type evaporator immersed in a still humid air environment with the presence of frost formation is carried out. In the numerical investigation, the suggested model considered the frost layer as a porous medium. The solution of a set of partial differential equations characterizing frost formation taking into consideration the variation of air ambient conditions during frost formation process and a diffusion term is preceded. In experimental investigation, the ambient air temperature is changed over a range of 20°C to 25°C and the relative humidity is varied from 41% to 56% while maintaining the plate type evaporator average temperature at nearly -10°C. Also, Rayleigh number was varied from 10^4 to $1.2x10^6$ and the dimensionless time from zero to 1. The results show that the system coefficient of performance decreases within a range of (10% - 15%), the average Nusselt number varies within a range of (15% - 30%) and the average Sherwood number varies within a range of (25% - 40%).

Keywords: frost formation, moisture, mass transfer**.**

NOMENCLATURE

A	Face area	**m^2**
Cp	Specific heat	kJ/kg.K
C	Concentration	kg/m^3
D	Diffusion coefficient	m^2/**s**
G	Gravity acceleration	**m/s^2**
H	Convective heat transfer coefficient	$W/m^2.K$
h_m	Mass transfer coefficient	m/s
I	Compressor current intensity	**A**
K	Thermal conductivity	W/m.K
L	Length of flat plat evaporator.	**m**
$\dot{m}$	Rate of mass collected from the cooled frost	kg/s
M	Mass of collected frost	**kg**
m"	Frost mass flux	kg/m^2
N	No. of measuring points on the surface (6 points)	**-**
P	Pressure	**N/m^2**
q″	Heat flux	kW/m^2
Q_{add}	Rate of heat added to the system	kW
Q_{loss}	Rate of heat loss from the system to the surrounding	kW
$Q_{tot.}$	Sum of rates of added and lost heat from the system	kW

T	The system collecting time duration	s
T_{air}	Ambient air temperature	K
$T_{f,s}$	Frost surface temperature	K
T_i	Plate surface temperature at point i	K
T_p	Flat plate average temperature	K
U	Velocity component in x-direction	m/s
V_c	Potential difference of the feeding current	V
V	Velocity component in y-direction	m/s
W_d	Input work of the compressor	kW
W_d	Average input work of the compressor	kW
X	X-coordinate	m
Y	Y-coordinate	m
y_f	Frost thickness	m
$y_{f,init.}$	Initial frost thickness	m
$L_{Solid.}$	Latent heat of solidification	kJ/kg
$L_{Liq.}$	Latent heat of condification	kJ/kg
$L_{Sub.}$	Latent heat of sublimation	kJ/kg
ΔT_{sens}	Sensible temperature difference	K
Greek Symbols		
B	Volumetric coefficient of thermal expansion	/١K
ρ_f	Frost density	kg/m^3
Δ	Quantity difference	-
N	Kinematic viscosity	m^2/s
T	Dimensionless time	-
Dimensionless Groups		
Nu	Nusselt number	$\frac{h A_l}{k}$
Pr	Prantdl number	$\frac{\nu}{\alpha}$
Ra	Rayleigh number	$\frac{\rho \beta g \Delta T A_l^3}{\alpha A \nu}$
Sh	Sherwood number	$\frac{h A_l}{D}$
τ	Dimensionless time	$t.\nu/L^2$
Sub-scripts		
A	Air	-
c,sat	Condensate at saturation	-
f,s	Frost surface	-
Nb	Neighbors of the given grid point Po	-
P	Flat plate	-
Sat	Saturation	-
∞	Ambient	-
Super-scripts		
˚	Flow rate	-
″	Flux	-

1. INTRODUCTION

In the developing world, refrigeration is used chiefly to store foodstuffs at low temperatures, thus inhibiting the destructive action of bacteria, yeasts, and molds. Whenever humid air comes in contact with a cooling coil, its temperature is below both the dew-point of air and the freezing point, frost will form. The nature of the frost forming on the coil will depend on the psychometric conditions prevailing inside the freezer and whether the air around the coil is sub-saturated or supersaturated. The processes involving heat transfer from a humid air stream to a plate, with simultaneous deposition of frost, are of great importance in a variety of refrigeration equipment. It was well recognized that frost formation on heat exchanger surfaces seriously affects the performance of a refrigeration system.

A lot of research work has been done to study the growth of frost on a cooling coil. Kennedy and Goodman [1], investigated frost formation on a vertical surface under natural convection conditions. Local heat and mass transfer coefficients from humid air to the frost surface with effective thermal conductivity and density of the frost were studied. The temperature distribution in the boundary layer adjacent to the frost surface allowed the calculation of the local values of the heat flux. Marinyuk [2], studied experimentally the effect of frost formation on heat transfer between a cylinder and its gaseous environment. The studied parameters were the total heat flux, the steady-state convective heat transfer coefficient, and the mass of frost adhering to the test cylinder. He concluded that thermal conductivity was the main emphasis of frost and the diffusion mechanisms of moisture transfer within the frost layer causes the frost density and thermal conductivity to increase with time. Östin and Andersson [3], studied the formation of frost on parallel horizontal plates facing a forced air stream at varying temperatures, relative humidity and air velocities. They found that both the surface temperature of the plates and the relative humidity of the air stream have important effects on the frost thickness. Also, the density of frost was found to increase with relative humidity and air velocity. A strip method was applied to determine the thermal conductivity and internal changes in the frost layer. They observed two categories of frost formation, monotonic and cyclic growth. The condensed water vapor contributed in equal amounts to increase in the thickness and the density while in the latter melting at the frost surface results in abrupt internal densification. Tao *et al.* [4], simulated frost deposition on a cold surface exposed to a warm moist air flow using a one- dimensional, transient formulation based on the local volume averaging technique. The spatial distribution of the temperature, ice-phase volume fraction (related to frost density) and rate of phase change within the frost layer were predicted. Their results indicated that the local effective vapor mass diffusivity was up to seven times larger than the molecular diffusivity of water vapor in air. Le Gal *et al.* [5], predicted a one-dimensional transient formulation to predict frost growth and densification on a cold wall submitted to a moist air flow. The model was based on a local volume averaging technique that allows the computation of temperature and density distributions throughout the entire frost layer according to time. The effective vapor mass diffusivity throughout frost should reach values several times larger than the molecular. Wu and Webb [6], conducted an experimental study to investigate the possibility of causing frost on a cold surface. Both hydrophilic and hydrophobic surfaces were examined. A thermo-electric cooler was used to provide a cooling source for the frosting surface. Fossa and Tanda [7], investigated experimentally and theoretically frost growth on a vertical plate in free convection and developed a simple model to predict frost growth key parameters (frost thickness, heat/mass transfer rates). The model had a good agreement with the experiments owing to the some simplifying assumptions made in the model (frost/air interface assumed to be flat, and the usage of simple relationships for frost properties). Cheng and Wu [8], investigated experimentally and theoretically the frost formation on a cold plate. Experimental observations were performed for the early stage of the frost growth process. It was found that the frost layer may exhibit a multiple-step ascending pattern in no more than 30 min which means that in a short time, the frost layer was possible to reach the frost layer full growth period under some certain environmental conditions, especially for the cases at higher air temperature, higher air humidity, or higher air velocity. Lee *et al.* [9], presented a mathematical model to predict the frost layer growth and the heat and mass transfer by coupling the air flow with the frost layer without employing experimental correlations. They dealt with the frost layer as a porous. The parameters considered in their search were the plate surface temperature and air conditions, such as air velocity, temperature, and absolute humidity and finally the frost surface temperature. Cheng and Shiu [10], investigated the frost formation on a cold plate in atmospheric air flow experimentally and theoretically. A microscopic image system was used to provide observations for the early stage of the frost growth process, record the pattern and the thickness of the frost layer per five seconds after the onset of frost formation. They observed a multiple-step ascending frost growth pattern caused by melting of frost crystals at the frost surface. The effects of velocity, temperature and relative humidity of air were studied with varied surface temperature of the cold plate. Shin *et al.* [11], investigated experimentally the effect of surface temperature on frost formation. Test samples with three different surfaces of which dynamic contact angles were 23, 55, and 88 deg were installed in a wind tunnel and exposed to a humid air flow. The air flow Reynolds number, humidity, the air and the cold plate temperatures were maintained at 9000, 0.0042 kg/kg dry air, 12°C and -22°C, respectively. The thickness and mass of frost layer were measured and used to calculate frost density while heat flux and temperature profile were measured to obtain thermal conductivity. Their results showed that the surface with a lower dynamic contact angle showed a higher frost density and thermal conductivity during a two-hour test. Lee and Yang [12], developed frost maps for two different surfaces having two different hydrophilic characteristics and to find ambient conditions associated with the formation of frost structures. They found that frost structures on surfaces with different direct contact angles are similar. However, low direct contact angle surface at low humidity provides (20–30%) denser frost formation due to the shift of areas with different structures. Yang and Lee [13], proposed a mathematical model to predict frost properties , heat and mass transfer within the frost layer formed on a cold plate. Laminar flow equations were employed for moist air and empirical correlations for local frost properties to predict the frost layer growth. Their results showed that the heat transfer coefficients obtained under non-frosting conditions are lower by 30% than those under frosting conditions and concluded that the air flow should be analyzed to obtain the accurate prediction for the frost growth. Lee and Ro [14], made a simple model on the assumption that the water-vapor concentration at the frost surface was saturated, and that the gradient of vapor pressure was the same as the value obtained from the (Clausius–Clapeyron) equation. Initial porosity of the frost layer affected the characteristics of frost growth and so modified the model with the assumption that the concentration of water-vapor at the frost surface was in super-saturation in order to solve the inconsistency of the diffusion resistance of water-vapor in the region of high porosity. Tso *et al.* [15], developed a model with two-phase flow for refrigerant coupled with a frost model for studying the behavior of an evaporator. They concluded that the formation of frost degrades the performance of the evaporator and that the air and wall temperature varies along the tubes and coil depth, which will lead to non-uniform frost growth with coil depth. Wu *et al.* [16], investigated experimentally frost formation on a horizontal copper. Their experiments showed that the frost formation on a cold surface generally began with the formation and growth of condensate droplets, freezing of the super-cooled condensate droplets, formation and growth of initial frost crystals on the frozen droplets, growth of frost crystals accompanied by the collapse of some of the crystals, and finally frost layer growth. Getu and Bansal [17], presented a theoretical model and experimental analyses of evaporators in frozen-food display cabinets at low temperatures in the supermarket industry. Their mathematical model adopted various empirical correlations of heat transfer coefficients and frost properties in a fin-tube heat exchanger in order to investigate the influence of indoor conditions on the performance of the display cabinets as it would be a good guide tool to the design engineers to evaluate the performance of supermarket display cabinet heat exchangers under various store conditions. Piucco *et al.* [18], advanced an investigation on the frost nucleation on flat surfaces as it focuses on the relevant parameters affecting the frost formation process, i.e., the surrounding air temperature and humidity, and the surface conditions (temperature, roughness and contact angle). Gupta *et al.* [19], presented a study of thermo-fluidic model developed for a domestic frost-free refrigerator. The governing equations, coupled with pertinent boundary conditions, are solved by employing a conservative control volume formulation, in the environment of a three-dimensional unstructured mesh. For the freezer compartment, the computationally predicted temperatures are somewhat higher than the experimental ones. Laguerre *et al.* [20], carried out experiments using a rectangular refrigerating cavity which can be more or less humidified and loaded with arranged cylinders. One of the vertical walls, made of aluminum, was kept at low temperature (+1ºC). They found that influence of water evaporation on air and cylinder temperatures is more pronounced at the bottom of the cavity.

In this work, a mathematical model is proposed and used to predict the frost formation and its growth accumulation on a flat plate heat exchanger. Heat and mass transfer coefficients and frost formation effect on the system performance are predicted. An experimental test rig is set up in a free air stream to validate the mathematical model.

2. THEORTICAL MODEL

In the present model, the moist air flows over a flat plate are shown in Figure (1) and frost layer is considered as a porous media. In order to predict the behavior of frost layer growth, it is assumed that all processes are unsteady and the variation of frost density in the direction normal to the horizontal cooling plate is negligible.

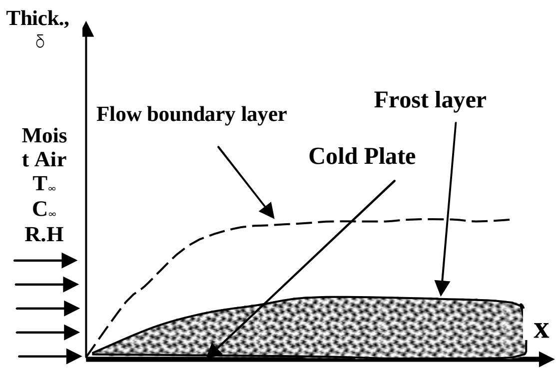

Fig.(1). Schematic diagram of theoretical model.

The governing equations are continuity, momentum, energy, and mass concentration assuming incompressible laminar flow with no viscous dissipation and using Boussinesqi approximation, these can be expressed as follows:

i. Continuity equation:

$$\frac{\partial u}{\partial x} + \frac{\partial v}{\partial y} = 0 \tag{1}$$

ii. Momentum equations:

$$\frac{\partial u}{\partial t} + u\frac{\partial u}{\partial x} + v\frac{\partial u}{\partial y} = -\frac{1}{\rho}\frac{\partial P}{\partial x} + v\left(\frac{\partial^2 u}{\partial x^2} + \frac{\partial^2 u}{\partial y^2}\right) \tag{2}$$

$$\frac{\partial v}{\partial t} + u\frac{\partial v}{\partial x} + v\frac{\partial v}{\partial y} = -\frac{1}{\rho}\frac{\partial P}{\partial y} + v\left(\frac{\partial^2 v}{\partial x^2} + \frac{\partial^2 v}{\partial y^2}\right) + g\,\beta(T - T_\infty) \tag{3}$$

iii. Energy equation:

$$\frac{\partial T}{\partial t} + u\frac{\partial T}{\partial x} + v\frac{\partial T}{\partial y} = \frac{k}{\rho\, C_p}\left(\frac{\partial^2 T}{\partial x^2} + \frac{\partial^2 T}{\partial y^2}\right) \tag{4}$$

iv. Mass concentration equation:

$$\frac{\partial c}{\partial t} + u\frac{\partial c}{\partial x} + v\frac{\partial c}{\partial y} = D\left(\frac{\partial^2 c}{\partial x^2} + \frac{\partial^2 c}{\partial y^2}\right) \quad (5)$$

v. The initial and boundary conditions

At the plate surface at (y=0)

$$at\ t = 0,\ u = 0,\ v = 0,\ T = T_w\ ,\ C = C_w \quad (6)$$

$$0 \leq x \leq L\ ,\ y = y_{f,int}\ ,C = C_{f,int}$$

Far from the surface at (y→∞)

$$\frac{\partial u}{\partial x} = 0\ ,\ v = 0\ ,\ T = T_w\ ,\ C = C_w \quad (7)$$

For Interface between the frost layer and air

$$\left(\frac{\partial T}{\partial y}\right)_{y=y_f} = \frac{k}{k_f}\left(\frac{\partial T}{\partial y}\right)_{y=y_f^*} + \frac{\rho L_{sub} D}{k_a}\left(\frac{\partial T}{\partial y}\right)_{y=y_f^*} \quad (8)$$

The previous equations can be solved to get the physical quantities heat and mass transfer coefficients and in turn Nusselt and Sherwood numbers as follows:

$$h = \frac{q''}{(T_{air} - T_p)} \quad \& \quad h_m = \frac{\Delta C''}{(\rho_{va} - \rho_{vf})} \quad (9)$$

Where q'' is the heat flux by the plate surface area, T_{air} is the temperature of the surrounding ambient air, T_p is that of the plate, Δc *is* the concentration flux of the collected frost and ρ_{va} is the vapor density at air temperature and ρ_{vf} is the vapor density at frost surface temperature.

$$Nu = \frac{h\,L}{k}, \qquad Sh = \frac{h_m\,L}{D} \quad (10)$$

Where L is the plate length, k is the thermal conductivity of air and D is the mass diffusivity of water vapor in air.

vi. Calculation of frost properties:

The water vapor transferred into the frost surface from moist air increases both the frost density (C_δ) and thickness (C_ρ). This phenomenon can be expressed as follows:

$$C_f = \frac{\rho D}{\Delta C}\left(\frac{\partial C}{\partial y}\right)_{\delta_f} = C_\delta + C_\rho \quad (11)$$

The mass flux for the frost density absorbed into frost layer is given by:

$$C_\rho = \int_{y=0}^{y=y_f}\left(\frac{D\ \rho_{vi}}{\Delta C}\right) dy \quad (12)$$

The frost density and thickness for each time interval are calculated as follows:

$$C_f^{t+\Delta t} = C_f^t + \left(\frac{C_\rho}{\rho_f\ y_f}\right)\Delta\tau \quad (13)$$

$$y_f^{t+\Delta t} = y_f^t + \frac{C_y}{\rho_f\ y_f} \quad (14)$$

The previous equations are solved using (CFD) Fluent 6.26 numerical technique.

3. EXPERIMENTAL TEST RIG

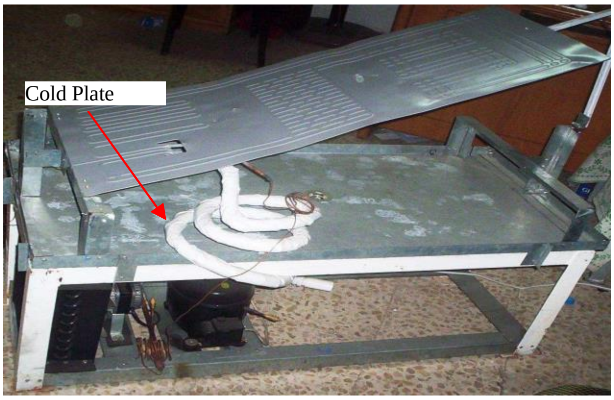

Fig.(2). Photo of the test rig components.

A photo of the test rig is presented in Figure (2). Figure (3) shows a schematic diagram for the details of the test rig. It consists of a simple refrigeration system with an easily tilted evaporator that is supported on an iron frame. The apparatus components are listed as follows: An evaporator flat plate (1) which is aluminum 980 mm 320 mm x 4 mm thickness and the flowing tubes which are punched through the plate. The evaporator is supported with two hinges at one side and riveted with a handle to help in tilting.

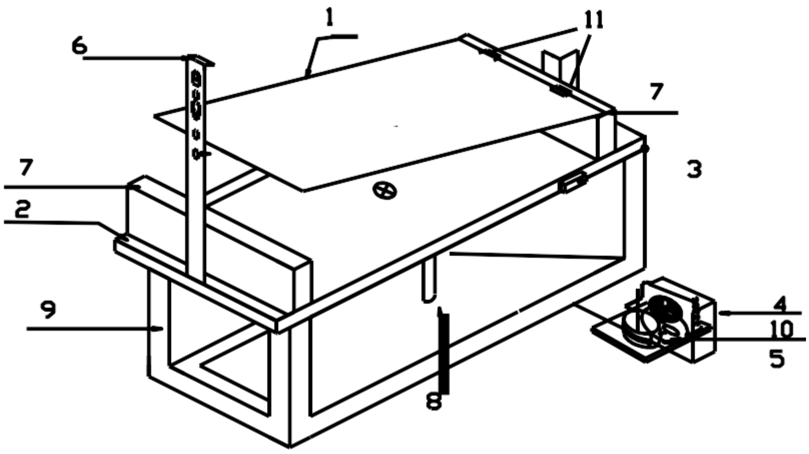

Fig.(3). Details of the test rig.

1. Evaporator
2. Drain enclosure
3. Thermostat
4. Air cooled condenser
5. Hermetic compressor
6. Level handlers
7. Evaporator seats
8. Drain hose
9. Apparatus body
10. Condenser fan
11. Tilt Hinges.

A drain pan (2) is made of a galvanized steel sheet (1160 x 550) mm, 1 mm thickness and height 5 mm. This enclosure supports the evaporator seats and collects the drainage of the melted ice from the evaporator. A thermostat (3) which is the main controller of the refrigeration cycle as it contains a bulb that is supported on the lower face of the evaporator. It has a range from (-30ºC / 30ºC) as it passes the electric current through the cycle only if it has not reached the required temperature. A condenser (4) which is an air cooled coil made of iron (270 mm x 270 mm x140 mm) with 5 rows and 3 columns of tubes.

A hermetic compressor (5) of 1/3 hp capacity and works on refrigerant R134a with a starting circuit and overload protection (power factor is 0.9). Two level steel handlers (6) 130 mm x 15 mm with holes for supporting the evaporator during its tilting. One of these is riveted to the plate and the other hinged to the evaporator seats (7). Evaporator seats are a pair of U-shaped galvanized steel pieces that are supported on the drain enclosure at the two ends of the evaporator. One includes the two tilting hinges and the other holds the plate when it is totally horizontal. Drain hose (8) is a flexible plastic hose that drains the melted frost from the two faces of the evaporator through the drainage tank. Apparatus frame (9) is made from iron 1130 mm x 460 mm x 400 mm. that includes the compressor, the condenser with its fan and the thermostat inside it and carries the evaporator with the drainage enclosure. Condenser fan (10) is an electric fan that is placed in one face of the condenser to help the heat transferring out of the condenser.

4. DATA REDUCTION

The frost formation mass flow rate (m˚) can be calculated for a time average as:

$$\dot{m} = \frac{m}{t} \tag{15}$$

Where, *m* is the mass of collected frost in grams and t is the time interval in seconds, The plate temperature can be calculated as the average temperature at different points on the plate as shown in Figure.(4).

$$T_p = \frac{\sum_{i=1}^{n} T_i}{n} \tag{16}$$

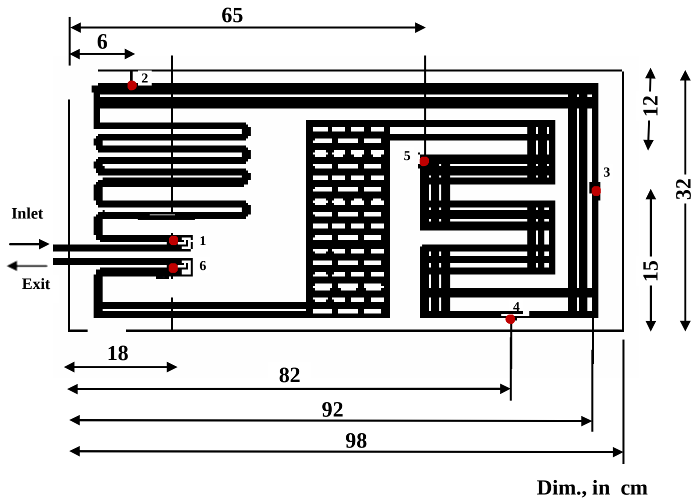

Fig.(4). Schematic diagram for the thermocouples position on the plate surface.

The quantity of heat added to the system (which is both sensible and latent) ($Q_{Add.}$) can be calculated as follows:

$$Q_{add} = \dot{m}\left[(Cp\Delta T_{sen})_v + L_{liq} + (Cp\Delta T_{sen})_s + L_{solid}\right] \qquad (17)$$

Where, $L_{Liq.}$ is the latent heat of liquefaction, C_p is the specific heat of water, L_{Solid} is the latent heat of solidification of water, $\Delta T_{sens.)v}$ is the sensible temperature difference between liquid water and freezing point and $\Delta T_{sens.)s}$ is the sensible temperature difference between freezing point and the frost surface temperature.

The rate of heat gain from the environment can be described as:

$$Q_{loss} = h_a A \Delta T_{sen} \qquad (18)$$

Where $h_{\mathbf{air}}$ is the convection heat transfer coefficient ($W/m^2.K$)**,** A is the evaporator surface area and $\Delta T_{loss.}$ is the Temperature difference between the frost and ambient temperature**.**

One can calculate the total capacity up the system as follows:

$$Q_T = Q_{add} + Q_{loss} \qquad (19)$$

The input power of the refrigeration system is that of the compressor which can be calculated as follows

$$\dot{W}_d = I V_c \cos \varphi \qquad (20)$$

Where I is the compressor current intensity, V is the potential difference of the feeding current and cos φ is the power factor.

The coefficient of performance of the system (COP) and heat flux q” are calculated from:

$$COP = \frac{Q_T}{\dot{W}_d} \qquad (21)$$

$$q'' = \frac{Q_T}{A} \tag{22}$$

Where q" is the heat flux .
The time average convective heat transfer coefficient (h) by dividing the heat flux by the temperature difference between ambient air and that of the plate as:

$$h = \frac{q''}{T_a - T_{f,s}} \tag{23}$$

Where $T_{f,s}$ is the frost surface temperature.

Nusselt number can be calculated as follows:

$$Nu = \frac{h\ L}{k} \tag{24}$$

Where L is the plate length and k is the thermal conductivity of air (W/m.K).

Similarly, one can calculate the time average mass transfer coefficient h_m by dividing the mass collected by both the plate surface area and the density difference between that of the water vapor at surrounding air temperature and that of just to be formed frost.

$$h_m = \frac{m}{A\left(\rho_{v,a} - \rho_{f,s}\right)} \tag{25}$$

And so Sherwood number can be calculated as follows:

$$Sh = \frac{h_m\ L}{D} \tag{26}$$

Where L is the plate length and D is the mass diffusivity of water vapor, and the moist air properties are calculated at bulk temperature between frost surface and air temperature.

5. MEASUREMENTS AND INSTRUMENTATION

5.1 Temperatures measurement

The temperature of the evaporator surface is measured by Copper – Constantan thermo-couples (T-type) of 0.5 mm as shown in Figure (4) (six thermocouples are glued into the surface of evaporator by high conductive glue (epoxy) and distributed on the surface). They are connected to the temperature recorder via a selector switch to the temperature recorder which has an accuracy of (**±0.**1°C).The surface temperature is considered to be the average temperature of al thermocouples readings.

5.2 Ambient temperature and relative humidity measurement

The ambient conditions that are measured by a thermo/hygrometer with range for temperature -10°C to 60°C ±(1°C) and for relative humidity 10 % to 99 % ±(3%)).

5.3 Frost mass measurement

A sensitive digital balance is used for measuring the mass of the formed frost on both sides of the evaporated surface after melting that are drained into the drain enclosure. The balance has a range from (0.2 – 300 g) and with an accuracy of (±1%).

5.4 Electric current intensity and potential difference measurement

The electric current intensity is measured by digital ammeter with the following specifications [range (0 - 10 Amp.± 1 %)] and the electric potential difference is measured by digital voltmeter the following specifications [range (0- 400 V ± 1%)].

6. EXPERIMENTAL ERROR ANALYSIS

The accuracy of the results obtained from experimental measurements is governed by the accuracy of the individual measuring devices. The maximum error in calculating heat transfer coefficient, mass transfer coefficient, Sherwood number are ±4.35%, ±6.5% and ±8.2% while the maximum error in calculating COP is about ±2%.

7. RESULTS AND DISCUSSION

7.1 Theoretical model results:

The theoretical results are illustrated for a two dimensional model using CFD (FLUENT 6.26) package. Figure (5) indicated that the average Nusselt number increases with increasing Rayleigh number until it reach the constant value at Rayleigh number up to 4×10^5 because the frost layer takes its maximum value and acts as insulation. Also, the average Nusselt number increases with increasing of Prandtle number.

Figure (6) shows that the average Sherwood number has the same trend of average Nusselt number with Rayleigh number. The average Sherwood number increases with increasing Rayleigh number. Also, the average Sherwood number slightly increases with increasing of Schmidt number.

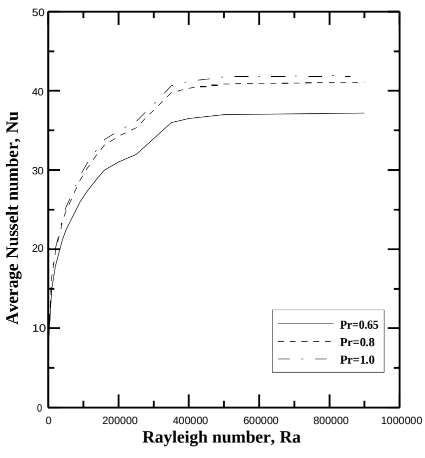

Fig.(5). Nusselt number versus Rayleigh number

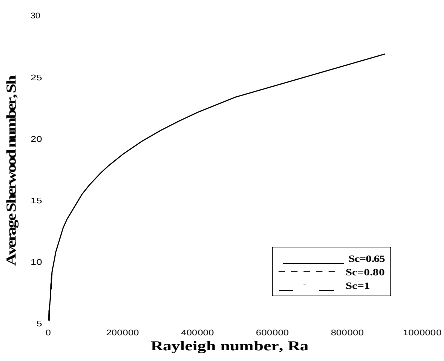

Fig.(6). Sherwood number versus Rayleigh number

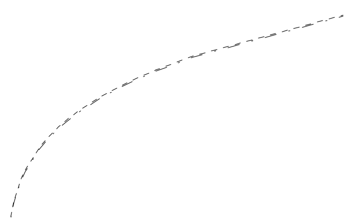

7.2 Effect of plate temperature:

From Figure (7), the air temperature at a plane 3 mm above the cold surface increases with the dimensionless distance (x_i/L). It is noted that at lower plate temperatures, the rate of increasing the air temperature is higher. Also, the air temperature increases for increasing plate temperature at a certain horizontal position.

The variation of local Nusselt number with dimensionless horizontal distance is shown in Figure (8). The local Nusselt number increases with the decreasing of the plate temperature.

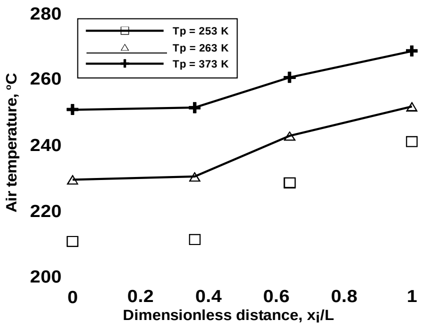

Fig.(7). Plate temperature distribution along the plate

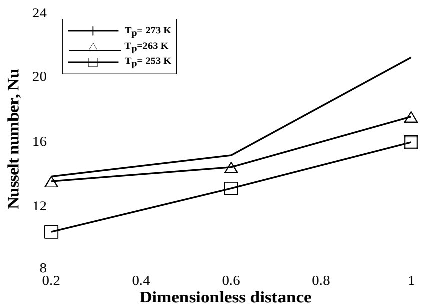

Fig.(8). Local Nusselt number vs position.

Figure (9), shows the plate temperature with dimensionless time ($\tau = \frac{t.\upsilon}{L^2}$) at different relative humidity. At a certain relative humidity, the plate temperature decreases with time. This decrease is due to the increase in the frost layer thickness which decreases the rate of heat transfer between the free air and the plate surface. The frost layer works as a growing insulator with time.

Figure (10) illustrates the relation between plate temperature and dimensionless time at different air temperature and fixed relative humidity of 52%. One can deduce that the plate temperature decreases with time due to the growth of frost layer.

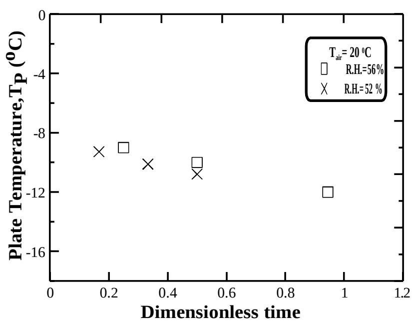

Fig.(9). Average plate temperature versus dimensionless time at varying relative humidity

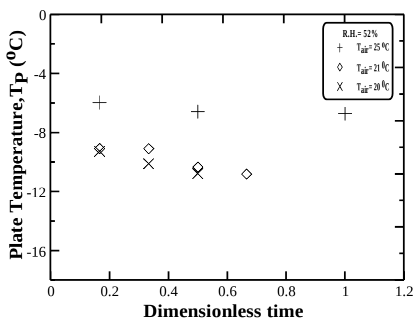

Fig.(10). Average plate temp., versus dimensionless time at varying air temperature

7.3 Validity of the model:

The average Nusselt number calculated from the present model is compared with that of the reference [13] for the same range of Rayeligh number at unity Prantdl number as shown in Figure (11). For the present and previous models the average Nusselt number increases with the increasing of Rayleigh number and takes the same trend.

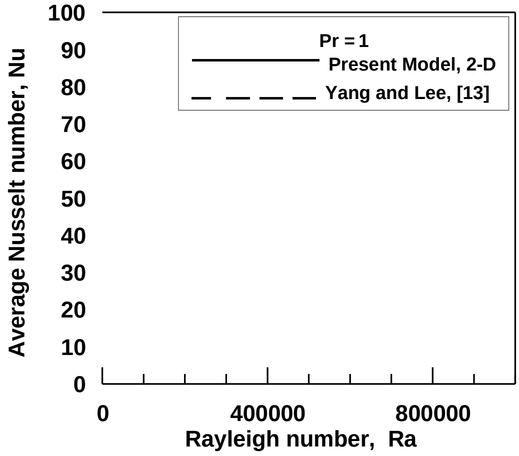

Fig.(11). Nusselt number versus Rayleigh number comparison.

8. EXPERIMENTAL RESULTS

The experimental results including plate temperature, frost collected mass, frost thickness, coefficient of performance of the system, heat and mass transfer coefficients, Nusselt and Sherwood numbers are demonstrated.

8.1 Plate temperature:

Figure (12) illustrates the plate temperature variation with dimensionless time, ($\tau = t.\nu/L^2$) at different relative humidity. One can recognize that at a certain relative humidity, the plate temperature decreases with time and this decreasing is due the increase in the frost layer thickness which decreases the rate of heat transfer between the free air stream and the plate surface. The frost layer works as a growing insulator with time. The higher the relative humidity, the higher the rate of this degradation can be observed.

Figure (13) shows the relation between plate temperature and dimensionless , ($\tau = t.\nu/L^2$) at different air temperature while relative humidity is 52%. It is deduced that the plate temperature decreases with both time due to the growing frost layer insulating process.

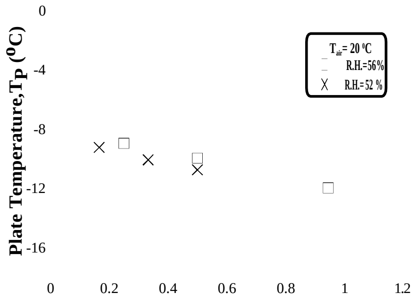

Fig.(12). Average plate temp., versus dimensionless time at varying relative humidity.

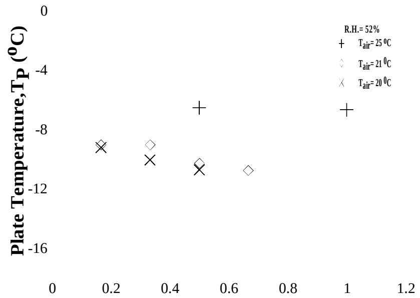

Fig.(13). Average plate temp., versus dimensionless time at varying air temperature.

8.2 Frost collected mass

Figure (14) illustrates the relation between frost mass collected (total mass from the plate) and dimensionless time, ($\tau = t.\nu/L^2$) at different relative humidity. One can observe that the increase of the collected frost mass with time which is reasonable due to the increase of the water vapor frosted from the air stream as the thickness and density of the frost layer increases with time. Also, it can be observed that the collected frost mass increases with the increase of the relative humidity for the same air temperature due to the increment of moisture content available in the same air stream subjected to be frosted on the plate.

Figure (15) illustrates the relation between frost mass collected and dimensionless time at different relative humidity. One can find that the frost mass collected increases with time at any air temperature. In a certain time the collected mass increases with increase of air temperature for the same relative humidity as the air moisture content increases and so the ability of changing a bigger part of it into frost is substantial.

8.3 Frost thickness:

One can illustrate that the relation between frost thickness and dimensionless time at different relative humidity from Figure. (16). It is noticeable that the frost thickness increases with time as the frost layer accumulates, Also, one can notice the higher increase in the frost thickness at higher air relative humidity for the same air temperature.

Figure (17) illustrates the relation between frost thickness and dimensionless time at different air temperature; one can deduce the increase of the frost layer with time and with air temperature as the frost layer accumulates due to the increase in the moisture content.

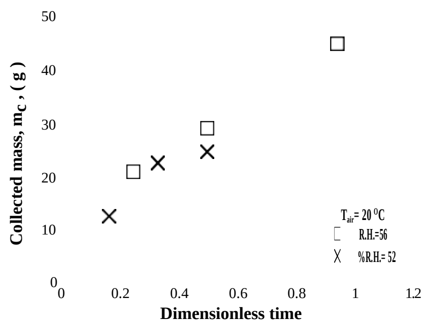

Fig. (14). The frost collected mass versus dimensionless time at Tair= 20OC.

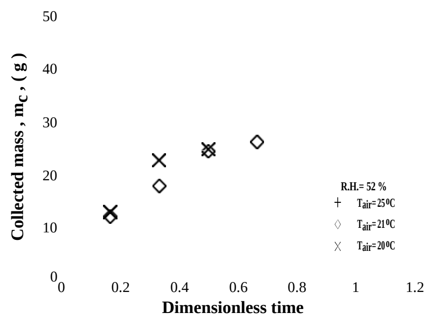

Fig.(15). The frost collected mass versus dimensionless time at R.H.=52%.

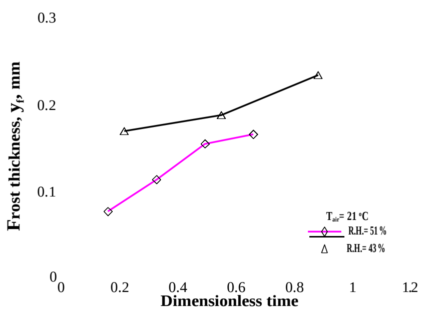

Fig.(16). The time average frost thickness and dimensionless time at Tair= 21 OC.

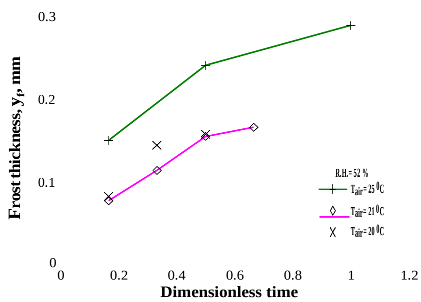

Fig.(17). The time average frost thickness and dimensionless time at R.H.= 52%.

8.4 Coefficient of performance

Figure (18) illustrates the relation between the average coefficient of performance and dimensionless time at different relative humidity; one can recognize the coefficient of performance decreasing with time for a range from (10-15%) due to the frost layer blockage and so degrading heat transfer process and so increasing the average compressor work done and increasing the frost thickness above the plate. Figure (19) illustrates the average coefficient of performance and dimensionless time at different air temperature; one can recognize that the decreasing of coefficient of performance is due to the growth of frost layer with time within a range of (10-15%). Due to the previously noted, frost layer blockage, the compressor workincreases.

8.5 Effect of dimensionless time on heat and mass transfer coefficients

Figure (20) illustrates the relation between the time average heat transfer coefficient and dimensionless time at constant air temperature. The heat transfer coefficient increases during

the early stage, while it decreases uniformly with time after that as the frost layer acts as heat transfer blocker.

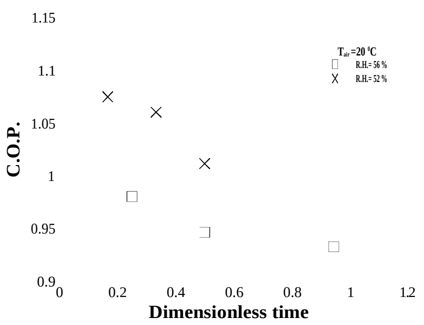

Fig. (18). The coefficient of performance versus dimensionless time at Tair= 20OC.

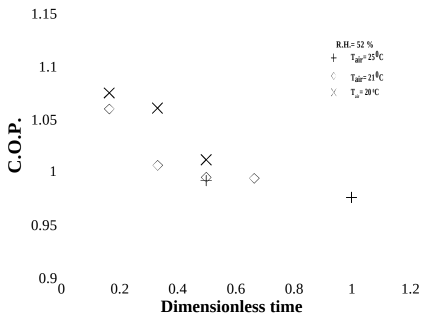

Fig.(19). The coefficient of performance versus dimensionless time at R.H.=52%.

Figure (21) illustrates the relation between the time average heat transfer coefficient and dimensionless time at constant relative humidity. The heat transfer coefficient increases uniformly with time, Also, the air temperature is inversely proportional to the heat transfer coefficient.

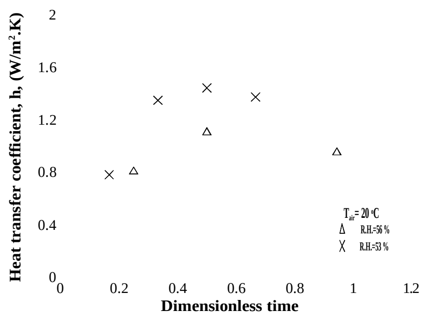

Fig.(20). Time average heat transfer coeff. versus dimensionless time at Tair= 20OC.

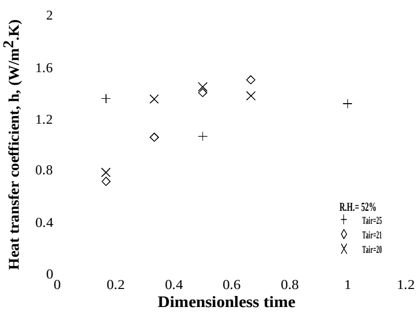

Fig.(21). Time average heat transfer coeff. and dimensionless time at R.H.=52%.

Figure (22) illustrates the relation between the mass transfer coefficient and dimensionless time at constant relative humidity at different air temperature. It is clear that the mass transfer coefficient increases uniformly with time and the lower the air temperature, the higher the mass transfer coefficient.

Figure (23) illustrates the relation between the mass transfer coefficient and dimensionless time, ($\tau = t.\nu/L^2$) at constant relative humidity at different air temperature. One can observe that the mass transfer coefficient increases uniformly with time and the lower the air temperature, the higher the mass transfer coefficient.

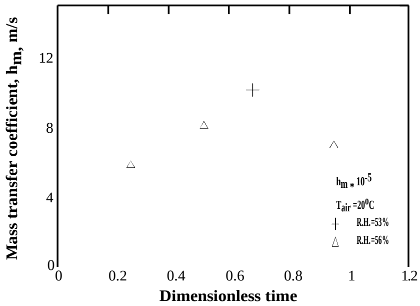

Fig.(22). Time average mass transfer coeff. versus dimensionless time at Tair= 20OC.

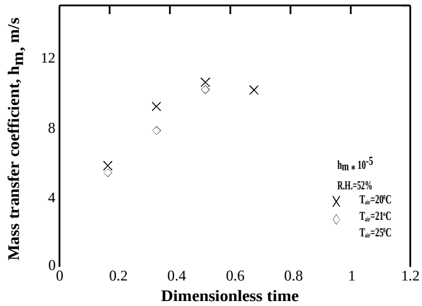

Fig.(23). Time average mass transfer coeff. versus dimensionless time at R.H.= 5.

8.6 Effect on dimensionless time on Nusselt and Sherwood numbers

Figure (24) illustrates Nusselt number and dimensionless time at constant air temperature and different relative humidity. It is observed that Nusselt number has the same trend of the heat transfer coefficient as Nusselt number increases during the early stage, while it decreases uniformly with time after that as the frost layer acts as heat transfer blocker.

Figure (25) illustrates the relation between Nusselt number and dimensionless time at constant relative humidity and different air temperature. The average Nusselt number increases uniformly with time and the air temperature is inversely proportional to the average Nusselt number.

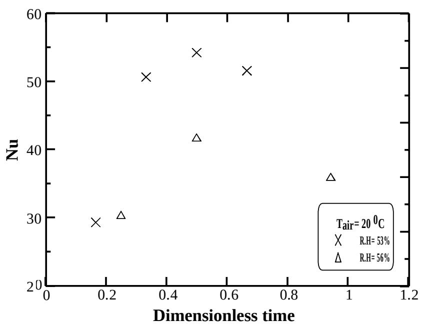

Fig.(24). Time average Nusselt number versus dimensionless time at Tair= 20OC.

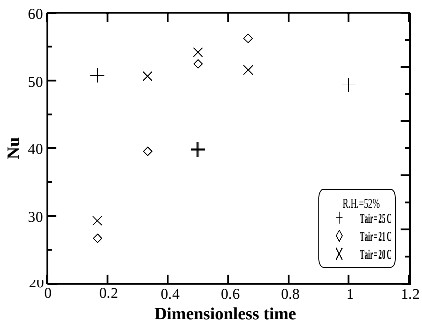

Fig.(25) . Time average Nusselt number versus dimensionless time at R.H.= 52%.

Figure (26) illustrates the relation between Sherwood number and dimensionless time at different relative humidity and ambient temperature of 20ºC. It is clear that Sherwood number increases uniformly with time and the lower relative humidity led to a significant decrease in Sherwood number. Figure (27) shows Sherwood number versus dimensionless time at constant relative humidity and different air temperature. It is clear that Sherwood number increases uniformly with time and the lower the air temperature, the higher Sherwood number.

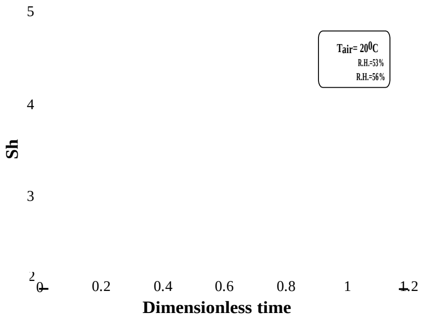

Fig.(26). Time average Sherwood number versus dimensionless time at Tair= 20 OC.

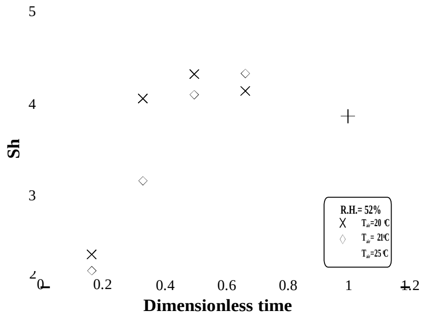

Fig. (27). Time average Sherwood number versus dimensionless time at R.H.=52%.

8.7 Comparison between present experimental and previous results

Figure (28) represents the mass of the frost accumulated variation with dimensionless time for the present experimental work and Gao *et al.*[21] numerical study at the same air temperature, relative humidity, and plate temperature .It is clear that the mass accumulated from the present model is higher than that of Gao *et al.*[21] and this is due the difference in the surface areas between the present and previous work.

Figure (29) represents the frost thickness variation with dimensionless time for present model and Gao *et al.*[21] at the same air temperature, relative humidity, and plate temperature. It is observed that the comparison between the two models shows a fairly in a good agreement.

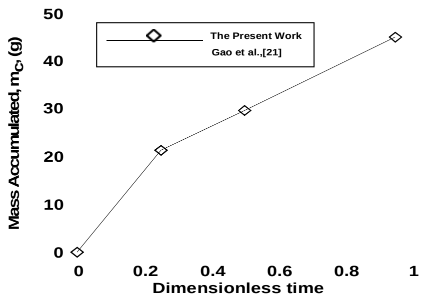

Fig.(28). Comparison between the present experimental data and the model of Gao *et al.* [21] for the collected mass.

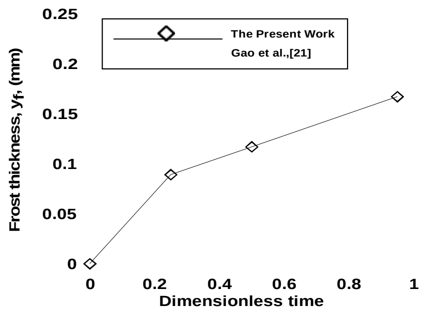

Fig.(29). Comparison between the present experiments and the model of Gao et.al. [21] of the frost thickness.

8.8 Heat and mass transfer correlations

The heat and mass transfer experimental results are correlated. The affecting parameters are the following: mass flow rate, the heat flux, the plate length, density, thermal conductivity, and temperature difference or thermal diffusivity. These correlations can be expressed as follows:

$$Nu = 2.46\ Ra^{0.21} \tag{27}$$

$$Sh = 2.01437\ Ra_m^{0.027057} \tag{28}$$

The correlations (27) and (28) are valid for; 10^4 <Ra < $1.2x10^6$ within error of ± 12% for Nusselt number and ± 10% for Sherwood number as shown in Figs.(30) and (31).

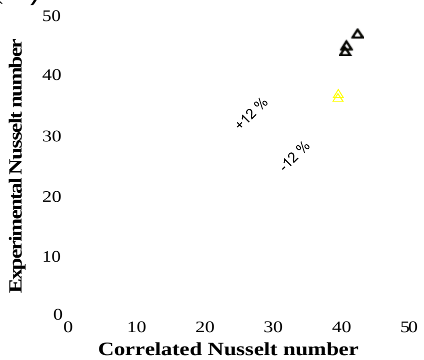

Fig.(30). Comparison of Nusselt number between the present experiments and the calculated results for (104 <Ra < 1.2x106).

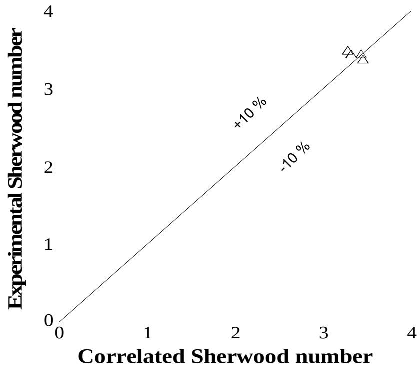

Fig.(31). Comparison of Sherwood number between the present experiments and the calculated results for (104 <Ra < 1.2x106).

8.9 Comparison between the present theoretical and experimental results:

Figure (32) shows the relation between theoretical and experimental average Nusselt number and Rayleigh number. One can observe that the average Nusselt number in both cases take the same trend but the experimental ones is higher than the theoretical; this is because of the assumptions of constant properties in the theoretical model.

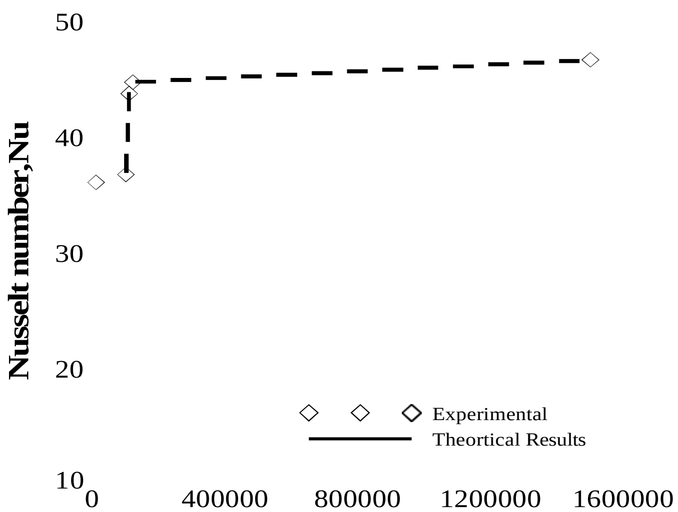

Fig.(32). Comparison between present theoretical and experimental results.

9. CONCLUSION

This study presents a mathematical model to predict the frost layer growth and the characteristics of its heat and mass transfer by coupling the air flow with the frost layer assuming the frost as a porous media. Also, the experimental facility is developed and constructed to investigate the frost growth process. The following remarks are concluded:

1- The frost layers accumulation causes degradation in the performance of the heat exchanger
2- The heat transfer coefficient is inversely proportional to the dimensionless time and accordingly Nusselt number.
3- Due to the degradation in the performance of the heat exchanger, subsequently the decrease in the COP will be significant as:
   - The system coefficient of performance decreases within a range of (10% - 15%).
   - The average Nusselt number varies within a range of (15% - 30%).
   - The average Sherwood number varies within a range of (25% - 40%).

10. REFERENCES

[1] Kennedy, L.A., and Goodman J., "Free Convection Heat and Mass Transfer Under Conditions of Frost Deposition", *Int. J. of Heat and Mass Transfer*, Vol. 17, No. 4, (1974), pp. 477-484.
[2] Marinyuk, B. T., "Heat and Mass Transfer under Frosting Conditions", *Int. J. of Refrigeration*, Vol. 3, No. 6, (1980), pp. 366-368.

[3] Östin, R. and Andersson, S., "Frost Growth Parameters in a Forced Air Stream "*Int. J. of Heat and Mass Transfer*, Vol. 34, No. 4-5, (1991), pp. 1009-1017.
[4] Tao, Y.X., Besant R.W. and Rezkallah K. S., "A Mathematical Model for Predicting the Densification and Growth of Frost on a Flat Plate" *Int. J. of Heat and Mass Transfer*, Vol. 36, No. 2, (1993), pp. 353-363.
[5] Le Gall, R., Grillot J. M. and Jallut, C., "Modeling of Frost Growth and Densification", *Int. J. of Heat and Mass Transfer*, Vol. 40, No. 13, (1997), pp. 3177-3187.
[6] Wu, X. M. and Webb, R. L., "Investigation of the Possibility of Frost Release From a Cold Surface", *Experimental Thermal and Fluid Science*, 24, No. 3-4, (2001), pp. 151-156.
[7] Fossa, M., and Tanda, G., "Study of Free Convection Frost Formation on a Vertical Plate", *J. of Experimental Thermal and Fluid Science*, Vol. 26, (2002), pp. 661–668.
[8] Cheng, C.H., and Wu, K. H., "Observations of Early-Stage Frost Formation on a Cold Plate in Atmospheric Air Flow", *J. of Heat Transfer*, Vol. 125, (2003), pp. 95-101.
[9] Lee, K.S., Jhee, S., and Yang, D., "Prediction of the Frost Formation on a Cold Flat Surface", *Int. J. of Heat and Mass Transfer*, Vol. 46, (2003), pp. 3789–3796.
[10] Cheng, C., and Shiu, C. "Oscillation Effects on Frost Formation and Liquid Droplet Solidification on a Cold Plate in Atmospheric Air Flow", *Int. J. of Refrigeration*, Vol. 26, (2003), pp. 69–78.
[11] Shin, J., Lee, H., Ha, S., Choi, B., and Lee, J., "Frost Formation on a Plate with Different Surface Hydrophilicity", *Int. J. of Heat and Mass Transfer*, Vol. 47, (2004), pp. 4881–4893.
[12] Lee, K. S., and Yang, D., "Dimensionless Correlations of Frost Properties on a Cold Plate", *Int. J. of Refrigeration*, Vol. 27, (2004), pp. 89–96.
[13] Yang, D., and Lee, K. S., "Modeling of Frosting Behavior on a Cold Plate", *Int. J. of Refrigeration*, Vol. 28, (2005), pp. 396–402.
[14] Lee, Y. B., and Ro, S. T., "Analysis of the Frost Growth on a Flat Plate by Simple Models of Saturation and Super Saturation", *J. of Experimental Thermal and Fluid Science*, Vol. 29, No. 6, (2005), pp. 685-696.
[15] Tso, C. P., Cheng, Y. C., and Lai, A. C. K., "Dynamic Behavior of a Direct Expansion Evaporator Under Frosting Condition, Part I. Distributed Model", *Int. J. of Refrigeration*, Vol. 29, (2006), pp. 611–623.
[16] Xiaomin, W, Wantian, D, Wangfa, X, and Liming, T., "Meso-scale Investigation of Frost Formation on a Cold Surface" *J. of Experimental Thermal and Fluid Science*, Vol. 31, (2007), pp. 1043–1048.
[17] Getu, M., and Bansal, P. K., "Modeling and Performance Analyses of Evaporators in Frozen-Food Supermarket Display Cabinets at Low Temperatures", *Int. J. of Refrigeration*, 30, No. 7, pp. 1227-1243.

[18] Piucco R. O., Hermes C. J. L., Melo, C., and Barbosa, J. R., "A Study of Frost Nucleation on Flat Surfaces", *Experimental Thermal and Fluid Science*, Vol. 32, No. 8, (2008), pp. 1710-1715.

[19] Gupta J. K., Gopal M., and Chakraborty, S., "Modeling of a Domestic Frost-free Refrigerator", *Int. J. of Refrigeration*, Vol. 30, (2007), pp.311-322.

[20] Laguerre O., Remy, D., and Flick, D., "Airflow, Heat and Moisture Transfers by Natural Convection in a Refrigerating Cavity", *J. of Food Engineering*, Vol. 91, (2009), pp. 197–210.

[21] Gao, B., Dong, Z., Cheng, Z., and Luo, E., "Numerical Analysis of the Channel Wheel Fresh Air Ventilator under Frosting Conditions", *HVAC Technologies for Energy Efficiency*, Vol. 4, (2006).

انتقال الحرارة وتكون الجليد على مبخر لوحي

جمال سلطان[١،٢]، السيد الشافعي[١]، محمد سعفان[١]، محمد عبد الرؤوف

[١] [illegible]

[٢] [illegible]

Email: gisultan@mans.edu.eg

[illegible]

ملخص البحث [illegible]